Silicon Photomultiplier-based Low-light *in vivo* Fiber Photometry

Mahrokh Namazi*, Govind Peringod†‡, Anupam Bisht§, Jaideep Bains†‡, Grant R Gordon†‡, Kartikeya Murari§*‡
* Dept. of Electrical and Software Engineering, † Dept. of Physiology and Pharmacology,‡ Hotchkiss Brain Insititute,
§ Dept. of Biomedical Engineering,
University of Calgary, Calgary, Canada
Email: kmurari@ucalgary.ca (Kartikeya Murari)

2023 IEEE Biomedical Circuits and Systems Conference (BioCAS) | 979-8-3503-0026-0/23/$31.00 ©2023 IEEE | DOI: 10.1109/BioCAS58349.2023.10389054

***Abstract*—Fiber photometry is an important tool for studying neural activity in freely moving animals. Existing systems utilize photodetectors requiring a high bias voltage or high optical power. The former results in expensive bulky systems and the latter leads to photobleaching or phototoxicity. We present a low-light fiber photometry system for recording neural activity in mice. Employing a sensitive silicon photomultiplier (SiPM) allows the use of low excitation light without requiring high-voltage power supplies. Isosbestic wavelength control was implemented to correct for motion artifacts. The same control signal was used as a novel method for SiPM gain correction, eliminating the need for additional sensors and control mechanisms. An off-the-shelf impedance measurement integrated circuit was used to simplify the electronics for homodyne detection of light. Sensitivity, dynamic range, and robustness to artifacts were characterized by measurement of fluorescence in fluorescein solutions. *In vivo* measurements during footshock experiments validated the system's effectiveness at 2.3 μW excitation power. The system's power requirements show promise for miniaturization and animal-mountable configurations.**

***Index Terms*—fiber photometry, neural recording, artifact reduction, SiPM, MPPC**

I. Introduction

Many aspects of neural activity, including neurotransmitter release, depend on intracellular calcium ions. Calcium indicators, like GCaMP, are fluorescent proteins that can bind to these ions. Consequently, their fluorescence is affected by changes in calcium level. Neural activity can be detected by measuring this fluorescence. In Ca^{+2}-sensitive fiber photometry using GCaMP probes, emission in response to optical excitation is recorded. Emission due to a main light source (470 nm) is modulated by neural activity. Additionally, a light source at the GCaMP isosbestic point (410 nm) is used as control. Since fluorescence at this wavelength is unaffected by neural activity, its variations simply represent motion artifacts. Therefore, the control signal can be used to correct for artifacts in the main signal [1].

Traditionally, fiber photometry systems use silicon photodiodes (Si PDs), photomultiplier tubes (PMTs), or CMOS cameras as photodetectors. Si PDs are used in commercial systems widely used by researchers. However, they exhibit limited sensitivity, and require high excitation powers in the range of tens of microwatts (μW) [2]–[4]. On the other hand, PMTs offer excellent gain ($10^6 - 10^7$) and have been employed in custom fiber photometry setups for low light detection [5]–[7]. PMTs come with drawbacks such as high cost, vulnerability to damage, and needing a supply voltage of hundreds of volts [6], [8], [9]. This makes them impractical for animal-mountable and low-power applications. CMOS cameras are relatively low-cost, but they have lower sensitivity and higher noise levels [1], [10].

Silicon photomultipliers (SiPMs) have emerged as potential alternatives to PMTs in various applications. SiPMs offer single-photon sensitivity at a lower cost compared to PMTs. They operate at a relatively low bias voltage ($\sim$25-75 V), and exhibit high gain ($\sim 10^6$) [5], [11]. Despite these advantages, their potential in fiber photometry has not yet been explored. One challenge associated with SiPMs is their gain's sensitivity to bias voltage and temperature [12]. Typically, SiPM gain stabilization is achieved by accurate temperature control or control of their bias voltage based on temperature sensing. This adds to the complexity and cost of the system [12]–[14].

We present an SiPM-based low-light fiber photometry system. Our system offers an affordable, sensitive, and convenient solution for studying neural activity. The electronics are based on an off-the-shelf impedance converter integrated circuit (AD5934, Analog Devices). AD5934 is designed for impedance measurement and is widely used exclusively for this purpose. However, with built-in data converters, analog conditioning and discrete Fourier transform (DFT) capability, it can simplify electronics for homodyne detection in various applications. An alternative approach for addressing SiPM's gain stability issues relying on fiber photometry's isosbestic control was used. To evaluate sensitivity and dynamic range, fluorescence of fluorescein isothiocyanate (FITC) solutions was measured. Robustness to temperature was demonstrated by measurement in the presence of a thermal perturbation. *In vivo* recordings in mice at 2.3 μW (470 nm) excitation resulted in data comparable to a commercial system using 13 times more excitation power.

II. System Architecture

The system consists of three main blocks: optics, electronics, and signal processing. As illustrated in Fig. 1, the electronics sinusoidally drive two light emitting diodes (LEDs) with wavelengths of 470 nm and 410 nm at 260 Hz and 280 Hz respectively. Each LED is associated with a signal path, one for the main channel (470 nm) and one for control (410 nm).

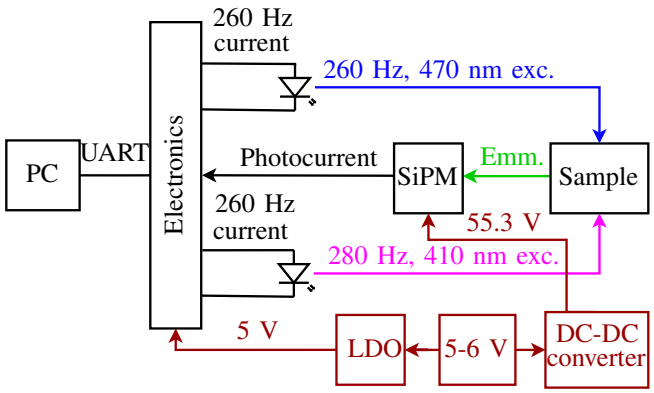

Fig. 1. Overall architecture of the proposed system.

The optics guide the LED output lights to a sample and direct the emission from the sample to an SiPM (S13360-1375PE, Hamamatsu). The resulting SiPM current is read out by the electronics and the data is sent to a PC for further processing. The electronics are implemented on a 6.5 cm × 3.8 cm printed circuit board which is powered by a 5-6 V supply. The optical components are contained within optical cage-mounts and lens tubes (Thorlabs). The material cost of the electronics is approximately 180 USD.

A. Optics

The output of two LEDs with wavelengths of 470 nm (XQEBLU, Cree LED) and 410 nm (QLUV04J3U, Quelighting Corp) are collimated by lenses (F240FC-A, Thorlabs) and filtered using bandpass filters (ET470/24m, Chroma and FB410-10, Thorlabs). A 425 nm high-pass dichroic beam splitter (DMLP425, Thorlabs) combines the two LED outputs. The combination of the two is incident on a 495 nm highpass dichroic beam splitter (T495lpxr, Chroma) which reflects both on to a lens (F240FC-A, Thorlabs) that couples light into a fiber optic patch cord for delivery to the sample. The resulting fluorescent light is collected by the patch cord and passes through the beam splitter and is filtered (ET525/50, Chroma) before being focused on to the SiPM (Fig. 2 (a-b)).

B. Electronics

The electronics consist of a microcontroller (PIC24FV16KM202, Microchip Technology), two impedance converters (AD5934), and signal-conditioning amplifiers (MCP642, Microchip Technology) interfacing with the SiPM and LEDs. The SiPM is biased at 52.61 V (over-voltage or excess voltage of 0.71 V) by the microcontroller DAC and a boost converter (TPS61391, Texas Instruments) powered by a 5-6 V unregulated voltage. All other electronics are powered by a 5 V regulated voltage (TC2054, Microchip Technology). Each of the two signal paths includes an impedance converter which generates a sinusoidal voltage. This voltage is then adjusted by a voltage amplifier (VA), and is input to a transconductance amplifier (TCA) driving an LED. The fluorescence-dependent SiPM photocurrent is converted to voltage by a transimpedance amplifier (TIA). The TIA output is fed back to both impedance converters to calculate the DFT at their respective excitation frequency. With a clock frequency of 1 MHz, each impedance converter samples its input voltage at 15625 Hz. DFT is calculated over 1024 samples collected over ∼65.5 ms, giving a DFT spectral resolution of ∼15 Hz. DFT data are obtained at a 10 samples per second rate. The data are read out by the microcontroller and sent to a computer via UART for further processing.

C. Signal Processing and Artifact Correction

The TIA output signal amplitudes corresponding to each excitation frequency (V_{470} and V_{410}) are calculated in MATLAB using the impedance converters' data.

The fluorescent emission in response to a 470 nm excitation consists of a baseline ($F_{470,b}$), affected by motion artifacts, and a calcium-dependent signal ($\Delta F_{470,Ca}$). Similar to $F_{470,b}$, the response to a 410 nm excitation (F_{410}) is only affected by artifacts, and the former can be approximated using the latter.

$$F_{470} = \Delta F_{470,Ca} + F_{470,b} \tag{1}$$

$$F_{470,b} \approx F_{410,scaled} = a.F_{410} + b \tag{2}$$

In fiber photometry, changes in calcium-dependent fluorescence are represented as $\Delta F/F$ [15].

$$\frac{\Delta F}{F} = \frac{\Delta F_{470,Ca}}{F_{470,b}} \approx \frac{F_{470} - F_{410,scaled}}{F_{410,scaled}} \tag{3}$$

Let A be the measurement system's overall gain. Then:

$$V_{470} = A \cdot (\Delta F_{470,Ca} + F_{470,b}) = \Delta V_{470,Ca} + V_{470,b} \tag{4}$$

From (2), $V_{470,b}$ can be expressed a function of V_{410}:

$$\begin{aligned} V_{470,b} \approx A \cdot (F_{410,scaled}) &= A \cdot (a \cdot F_{410} + b) \\ &= a \cdot V_{410} + A \cdot b \end{aligned} \tag{5}$$

If $|b| << |a \cdot F_{410}|$, $V_{470,b}$ can be approximated as $a \cdot V_{410}$. The coefficient a can be obtained by fitting a linear regression model to the recordings in a stimulus-free set of data where $V_{470} \approx V_{470,b}$. Then $\Delta F/F$, can be calculated as follows:

$$\begin{aligned} \frac{V_{470} - a \cdot V_{410}}{a \cdot V_{410}} &\approx \frac{V_{470} - V_{470,b}}{V_{470,b}} \\ &= \frac{\Delta V_{470,Ca}}{V_{470,b}} = \frac{\Delta F}{F} \end{aligned} \tag{6}$$

Therefore, SiPM gain variations do not affect the calculated fluorescence, because gain was monitored by the control channel and accounted for in the calculation.

III. Experimental Results

A. Characterization

With a 6 V supply, during measurement, the circuit draws 56 mA of current of which 34 mA is consumed by the impedance converters, 3 mA by the LEDs, 5 mA by the boost converter, 2 mA by the LDO, and 12 mA by the microcontroller and the analog front-end.

The excitation light was measured by a detector (PDA36A2, Thorlabs) and recorded by a DAQ device. Fig. 3 (a) shows the

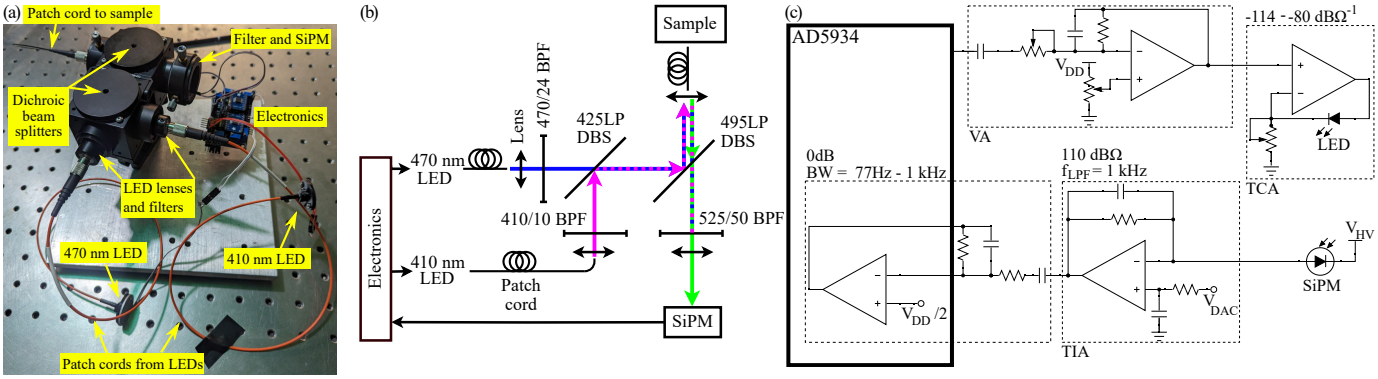

Fig. 2. The fluorescence measurement setup. (a) A photo of the setup. (b) Block diagram of the optics. BPF: bandpass filter, DBS: dichroic beam splitter. (c) Schematics of the analog electronics for one channel. VA: voltage amplifier, TCA: transconductance amplifier, TIA: transimpedance amplifier, V_{HV}: boost converter output, V_{DAC}: microcontroller digital to analog converter output. The VA is AC coupled to the impedance converter's (AD5934) output and has a cut-off frequency of 1 kHz. Its passband gain can be set to -23 to 10 dB.

signal in the frequency domain. Total harmonic distortions of 0.6% and 5.4% were observed for the 260 Hz and 280 Hz channels respectively. The excitation wavelength spectrum, measured by a spectrometer shows peak excitation wavelengths of 410 nm and 470 nm (Fig. 3 (b)).

To observe noise in the measurement stage, the SiPM was shielded from light. Under dark conditions, the impedance converter's op-amp's output represents noise at the ADC's input. The noise was $\sim$582 μV_{rms} and the spectrum is shown in Fig. 3 (c). With a 5 V supply, the 12-bit ADC's least significant bit is 1.22 mV which is 2.1 times the analog noise.

B. Fluorescence and Gain Stabilization

Fluorescence of FITC solutions were measured using the custom fiber photometry system. The 470 and 410 nm LEDs were driven to mean optical powers of 3.80 μW and 3.92 μW respectively to excite the samples. Fig. 4 (a) shows the TIA output voltage during measurement in a 0.25 μM solution. After calculating fluorescence, the data was scaled to represent concentration of FITC. A one-minute reconstructed fluorescence signal from the same sample is shown in Fig. 4 (b), where output represents fluorescence. A rise in temperature was induced by briefly touching the back of the SiPM board. This decreases the SiPM gain, causing a dip in both main and control signals. Correction stabilizes the output. To evaluate the signal's stability, signal to noise ratio (SNR) was calculated. SNR is defined as μ/σ, where μ is the mean and σ is the standard deviation of the signal. Correction improved SNR from 113 to 387. In another measurement with no thermal perturbation, an SNR of 371 was observed. This indicates the system's robustness to temperature variations.

Fluorescence of six FITC solutions with concentrations of 6.25 nM to 0.4 μM was measured (Fig. 4 (c)). In the 25 nM to 0.4 μM range, the output linearly changes with concentration, with a root mean square percentage error of 3.4%. In *in vivo* fiber photometry changes of 5% to 80% with reference to a baseline are of interest. This baseline varies among different animals. Based on *in vivo* recordings and measurement of FITC solutions with a commercial setup (Doric Lenses), for

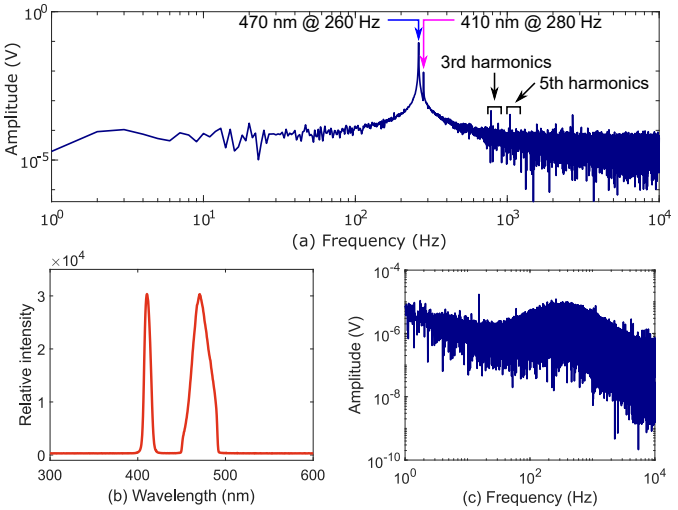

Fig. 3. Characteristics of the excitation light and the sensing stage. (a) Excitation light, measured by an amplified detector, in frequency domain. Harmonics, up to the fourth, are marked with arrows. (b) Excitation wavelengths. (c) Output of the impedance converter's op-amp under dark conditions.

the targeted animals in this study, this baseline is equivalent to 0.2 μM to 0.3 μM FITC solutions. Sensitivity to small changes in fluorescence at this operating point was evaluated by diluting a 0.26 μM solution by 1% in four steps and measuring fluorescence at these five concentrations. Contrast to noise ratio (CNR, defined below) was calculated as a measure of sensitivity.

$$CNR = \frac{|\mu_2 - \mu_1|}{\sqrt{\frac{1}{2}(\sigma_2^2 + \sigma_1^2)}} \tag{7}$$

Where μ and σ are as defined earlier and the subscripts indicate different concentrations. The average CNR in these four steps was 4.30. A CNR of 2 means the change in mean is twice the standard deviation of the signal. Defining a CNR of 2 as the minimum detectable change, changes as small as 0.46% can be detected at this baseline.

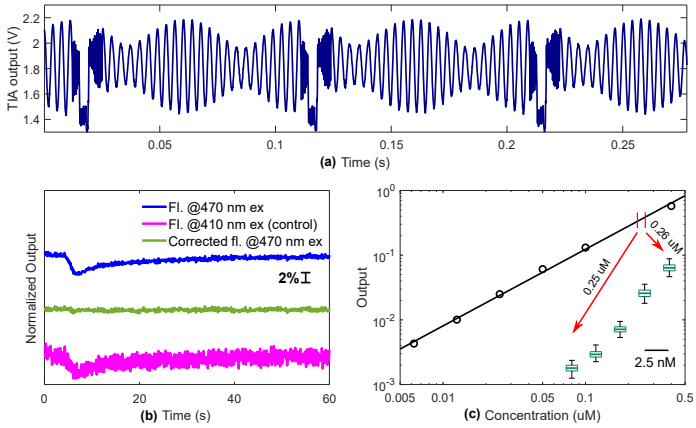

Fig. 4. Fluorescence measurements in FITC solutions. (a) TIA output voltage during measuring a 0.25 μM solution. Sinusoidal excitation stops during serial communication and calculations. (b) Correction of temperature-dependent SiPM gain variation during measuring a 0.25 μM solution. An increase in temperature causes a decrease in perceived fluorescence (Fl.) in response to the 470 nm (main) and 410 nm (control) excitations. The corrected signal is robust to temperature change. (c) Fluorescence of 6.25 nM to 0.4 μM FITC solutions. The boxplots show mean, standard deviation, maximum, and minimum in 5 concentrations between 0.25 μM and 0.26 μM.

C. *In vivo* Experiments

All animal procedures were approved by the University of Calgary's Animal Care and Use Committee. Four-six weeks before recordings, transgenic mice expressing the fluorescent protein GCaMP6f in neurons (animal 1) or astrocytes (animal 2) were implanted with a fiber-optic cannula targeting the hypothalamic paraventricular nucleus. Prior to experiments, animals were handled for 5-10 minutes for 3 consecutive days and then habituated to the recording environment and to the fiber tether for 20 minutes for 2 more days.

Mice were placed in a footshock cage, where they experienced ten 2-second shocks occurring every 30 seconds. These experiments were conducted on two mice twice; first with the custom setup and then with a commercial setup (Doric Lenses). In the custom setup the 470 nm and 410 nm LEDs were driven to mean optical powers of 2.3 μW and 1.7 μW, while in the commercial setup they were driven to 30 μW and 7.1 μW respectively. The results are depicted in Fig. 5.

The commercial setup exhibited better sensitivity to neural activity, since in both subjects, the average peak increase in $\Delta F/F$ due to footshocks was 2-2.6 times larger than that from the custom setup, while the standard deviation in a stimulus-free section was slightly lower. Smaller peaks may be due to the small difference between the excitation frequencies compared to the DFT resolution. This can cause crosstalk between the two channels and lead to overcorrection. The mean baseline in the first and last 10 seconds of recordings were compared. The baseline decrease was larger for the commercial setup. In the case of animal 1, this decrease was 10 times larger. This may be due to photobleaching caused by a high excitation power.

In the presented preliminary *in vivo* experiments, conservative gain settings were employed to ensure proper functionality

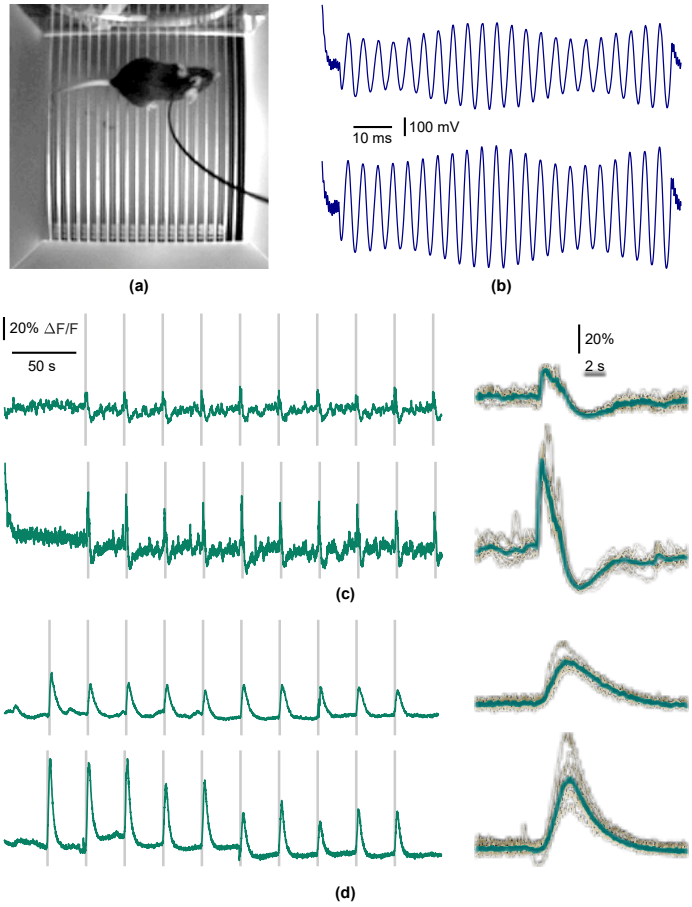

Fig. 5. *In vivo* fluorescence measurement. (a) A mouse inside a footshock cage with the patch cord connected. (b) TIA output before (top) and at time of peak response (bottom) applying a footshock to animal 1. (c) Animal 1's response to ten footshocks recorded by the custom setup (top) and the commercial setup (bottom) and the average footshock response. (d) same as (c) for animal 2.

without saturation. Based on these initial results, there is potential to enhance the system's performance by increasing the sensor read-out gain, optimizing SiPM biasing for improved gain to dark count ratio, and using more widely separated excitation frequencies. Through these optimizations, enhanced sensitivity, a higher SNR, and lower excitation powers may be possible. While the focus of this study was primarily on using low optical power, low-power implementation of electronics is feasible due to the SiPM biasing and the optical power requirements. This enables the development of a low-power animal-mountable device.

IV. Conclusions

A cost-effective low-light fiber photometry system for recording neural activity in mice was presented. By utilizing an SiPM, neural activity was detected using low excitation light without requiring high-voltage power supplies. The system's power requirements open up possibilities for miniaturization and animal-mountable configurations. Overall, our fiber photometry system offers researchers a convenient and reliable tool for studying neural dynamics in freely moving animals.

REFERENCES

[1] E. Martianova, S. Aronson, and C. D. Proulx, "Multi-fiber photometry to record neural activity in freely-moving animals," Journal of Visualized Experiments, no. 152, 2019. doi:10.3791/60278

[2] "Newport Visible Femtowatt photoreceiver module," Doric Lenses Inc., https://neuro.doriclenses.com/products/newport-visible-femtowatt-photoreceiver-module (accessed Jun. 11, 2023).

[3] A. Sengupta et al., "Basolateral amygdala neurons maintain aversive emotional salience," The Journal of Neuroscience, vol. 38, no. 12, pp. 3001–3012, 2017. doi:10.1523/jneurosci.2460-17.2017

[4] L. Yang, K. Lee, J. Villagracia, and S. C. Masmanidis, "Open source silicon microprobes for high throughput neural recording," Journal of Neural Engineering, vol. 17, no. 1, p. 016036, 2020. doi:10.1088/1741-2552/ab581a

[5] A. Sengupta et al., "Basolateral amygdala neurons maintain aversive emotional salience," The Journal of Neuroscience, vol. 38, no. 12, pp. 3001–3012, 2017. doi:10.1523/jneurosci.2460-17.2017

[6] K. Simone, T. Füzesi, D. Rosenegger, J. Bains, and K. Murari, "Open-source, cost-effective system for low-light in vivo fiber photometry," Neurophotonics, vol. 5, no. 02, p. 1, 2018. doi:10.1117/1.nph.5.2.025006

[7] Z. Liang, Y. Ma, G. D. R. Watson, and N. Zhang, "Simultaneous GCAMP6-based fiber photometry and FMRI in rats," Journal of Neuroscience Methods, vol. 289, pp. 31–38, 2017. doi:10.1016/j.jneumeth.2017.07.002

[8] Hamamatsu Photonics K.K Editorial Committee, Photomultiplier Tubes - Basics and Applications, 4th ed., Hamamatsu Photonics K.K Electron Tube Division, 2017.

[9] E. Anisimova et al., "Mitigating radiation damage of single photon detectors for space applications," EPJ Quantum Technology, vol. 4, no. 1, 2017. doi:10.1140/epjqt/s40507-017-0062-z

[10] M. N. Khiarak et al., "A Wireless Fiber Photometry System Based on a High-Precision CMOS Biosensor With Embedded Continuous-Time $\Sigma\Delta$ Modulation," in IEEE Transactions on Biomedical Circuits and Systems, vol. 12, no. 3, pp. 495-509, June 2018, doi: 10.1109/TBCAS.2018.2817200.

[11] B. Dolgoshein et al., "Status report on Silicon Photomultiplier Development and its applications," Nuclear Instruments and Methods in Physics Research Section A: Accelerators, Spectrometers, Detectors and Associated Equipment, vol. 563, no. 2, pp. 368–376, 2006. doi:10.1016/j.nima.2006.02.193

[12] D. Zhang et al., "Gain stabilization and consistency correction approach for multiple SiPM-based gamma-ray detectors on GECAM," Nuclear Instruments and Methods in Physics Research Section A: Accelerators, Spectrometers, Detectors and Associated Equipment, vol. 1027, p. 166222, 2022. doi:10.1016/j.nima.2021.166222

[13] R. R. Raylman and A. V. Stolin, "Immersion cooling of Silicon Photomultipliers (SiPM) for Nuclear Medicine Imaging Applications," Radiation Measurements, vol. 85, pp. 111–115, 2016. doi:10.1016/j.radmeas.2015.12.043

[14] F. Licciulli and C. Marzocca, "An active compensation system for the temperature dependence of SIPM gain," IEEE Transactions on Nuclear Science, vol. 62, no. 1, pp. 228–235, 2015. doi:10.1109/tns.2015.2388580

[15] C. A. Bruno et al., "pMAT: An open-source software suite for the analysis of fiber photometry data," Pharmacology Biochemistry and Behavior, vol. 201, pp. 173093, 2021. doi:10.1016/j.pbb.2020.173093